Journal of Applied Physics ARTICLE scitation.org/journal/jap

Power matching to pulsed inductively coupled plasmas

Cite as: J. Appl. Phys. **127**, 133302 (2020); doi: 10.1063/5.0002522
Submitted: 25 January 2020 · Accepted: 19 March 2020 ·
Published Online: 6 April 2020

View Online Export Citation CrossMark

Chenhui Qu,[1,a)] Steven J. Lanham,[2,b)] Steven C. Shannon,[3,c)] Sang Ki Nam,[4,d)] and Mark J. Kushner[1,e)]

AFFILIATIONS

[1]Department of Electrical Engineering and Computer Science, University of Michigan, Ann Arbor, Michigan 48109-2122, USA
[2]Department of Chemical Engineering, University of Michigan, Ann Arbor, Michigan 48109-2136, USA
[3]Department of Nuclear Engineering, North Carolina State University, Raleigh, North Carolina 27695-7909, USA
[4]Mechatronics R&D Center, Samsung Electronics Co., Ltd., 1-1 Samsungjeonja-ro, Hwaseong-si, Gyeonggi-do 18448, South Korea

[a)]chenqu@umich.edu
[b)]sjlanham@umich.edu
[c)]scshanno@ncsu.edu
[d)]sangki.j.nam@samsung.com
[e)]**Author to whom correspondence should be addressed:** mjkush@umich.edu

ABSTRACT

Matching of power delivery to nonlinear loads in plasma processing is a continuing challenge. Plasma reactors used in microelectronics fabrication are increasingly multi-frequency and/or pulsed, producing a non-linear and, in many cases, non-steady state electrical termination that can complicate efficient power coupling to the plasma. This is particularly the case for pulsed inductively coupled plasmas where the impedance of the plasma can significantly change during the start-up-transient and undergo an E–H (capacitive-to-inductive) transition. In this paper, we discuss the results from a computational investigation of the dynamics of power matching to pulsed inductively coupled plasmas (Ar/Cl_2 mixtures of tens of mTorr pressure) using fixed component impedance matching networks and their consequences on plasma properties. In this investigation, we used set-point matching where the components of the matching network provide a best-case impedance match (relative to the characteristic impedance of the power supply) at a chosen time during the pulsed cycle. Matching impedance early during the pulse enables power to feed the E-mode, thereby emphasizing capacitive coupling and large excursions in the plasma potential. This early power coupling enables a more rapid ramp-up in plasma density while being mismatched during the H-mode later in the pulse. The early match also produces more energetic ion bombardment of surfaces. Matching late in the pulse diminishes power dissipated in the E-mode at the cost of also reducing the rate of increase in plasma density.

I. INTRODUCTION

The combined impedance of the reactor and the plasma in low pressure plasma processing for microelectronics fabrication, using both capacitively and inductively coupled plasmas (ICPs), is typically non-linear.[1,2] Common combined impedances can range from 100s of mΩ to 100s of Ω and up to kilo-ohms of reactance. These conditions make it difficult to deliver power to the plasma from conventional power supplies and transmission lines that typically have fixed impedances of 50–75 Ω. The power reflection coefficient, Γ_R, is the power reflected from the plasma reactor relative to the power delivered by the power supply through a transmission line (typically a coaxial cable) to the plasma reactor. The reflection results from the output impedance of the power supply and the transmission line differing from that of the plasma reactor,

$$\Gamma_R = \frac{Z_L - Z_0}{Z_L + Z_0}, \qquad (1)$$

where Z_L is the impedance of the load (in this case, the combined impedance of the plasma reactor and the plasma) and Z_0 is the output impedance of the power supply and the transmission line.[3] Since Z_L has reactive contributions, Γ_R typically has both real and imaginary components from which both the magnitude and the relative phase of the forward and reflected waves can be determined. Typically, only the magnitude of reflection $|\Gamma_R|$ is used to characterize the matching efficiency.

The usual remedy to maximize power transfer to a plasma processing reactor (and minimize reflection) is to employ an impedance matching network (IMN) between the transmission line and the plasma reactor.[4–6] The IMN usually contains reactance (capacitors and inductors) both in series and in parallel to the load with the goal of making the input impedance to the IMN be the same as the power supply termination impedance and transmission line impedance. In doing so, the reflection coefficient is minimized. In practice, impedance matching is complicated by both the non-linear characteristics of the plasma and the increasingly common use of multiple frequencies and pulsed power. Even if driven with a single frequency, the non-linear response of the plasma to that single frequency power will produce higher harmonics in current, thereby making reproducible impedance matching more challenging.[7,8]

The use of pulsed power further complicates matching as the plasma contribution to Z_L can change by orders of magnitude during the pulsed cycle. For example, pulsed ICPs as used in microelectronics fabrication operate at pressures of tens of mTorr in attaching gas mixtures such as Ar/Cl_2 powered with radio frequency (RF) supplies of a few to tens of MHz. The pulsed repetition frequency (PRF), pulses per second, can be hundreds of Hz to tens of kHz. Duty cycle (DC), the fraction of time the power is applied per cycle, can be 10%–50%. The end result is that the electron density at the time the power is applied at the leading edge of the pulse can be as low as $10^8\ \mathrm{cm}^{-3}$, whereas later during the pulse, the electron density can exceed $10^{11}\ \mathrm{cm}^{-3}$.[9,10] These densities can increase across these three decades during a few to tens or hundreds of μs depending on the power delivery system and reactor design. The reactor contribution to Z_L for an ICP is typically dominated by the positive reactance of the inductance of the antenna, though the antenna will also have resistance.

Z_L for a pulsed ICP has additional dynamics due to the E-to-H (capacitive-to-inductive) transition that occurs during the transient in plasma density at the beginning of a pulsed period.[11–15] If the electron density at the beginning of a power pulse is too low, the electromagnetic skin depth, λ_S, may exceed the dimensions of the reactor, which then makes inductive coupling of power from the antenna problematic. For these conditions, the antenna simply acts as an electrode that electrostatically and capacitively couples power into the plasma through the dielectric window between the antenna and the plasma.[11] This is the E-mode during which power can be dominantly coupled into the plasma by sheath oscillation (much like a capacitively coupled plasma) with power mainly deposited by ion acceleration from the plasma into the dielectric window under the antenna.[15] During the capacitive E-mode, the reactance of the plasma is negative. As the electron density increases, λ_S decreases, which increases the fraction of power that is inductively coupled until the power is dominantly delivered by electron acceleration in the electromagnetic field within λ_S of the window. This is the H-mode during which the reactance of the plasma is positive. In practice, there may be mixed-mode coupling, both E-mode and H-mode during quasi-steady state operation of the ICP.[11,12] The degree of E- and H-mode coupling depends on factors such as the voltage across the antenna, the proximity of the antenna to the window, the shape of the antenna, gas pressure and composition, and the use of a Faraday shield between the antenna and plasma.[16]

The E–H transition in ICPs has been addressed both experimentally and theoretically.[17–25] When measuring the electron energy distribution (EED), Chung and Chang found that during the E-mode, the EED evolves from a bi-Maxwellian to a Druyvestein-like structure when increasing pressure.[26] During the H-mode, having a significantly larger electron density with a higher rate of e–e collisions, the EED remains essentially as a Maxwellian. To smoothen the severity of the E–H transition, Singh and Pargmann investigated the use of a Faraday shield to minimize capacitive coupling from the antenna.[16] When using the Faraday shield, the plasma potential at low power was lower, indicating lower capacitive coupling while the electron density was also lower. During the H-mode, the antenna current and voltage decreased when using the Faraday shield. Had the plasma been operating purely in the H-mode, there would not have been a decrease in current when using the Faraday shield, which then implies that even in the H-mode, there was mixed E- and H-mode coupling.

Kempkes *et al.* investigated the effect of the power modulation on the E–H transition using rectangular and triangular power waveforms.[27] They found that even with smoothly varying power (triangular waveform), abrupt E–H transitions occurred. Kawamura *et al.* performed two-dimensional (2D) simulations by E–H transitions in ICPs sustained in Cl_2.[28] They found ionization instabilities and modulations in electron density attributed to rapid transitions between E- and H-modes.

The E–H transition often displays hysteresis behavior. The transition between the low E-mode electron density to the high H-mode electron density occurs at different powers when the power is increased (occurs at high power) or decreased (occurs at low power). The power deposition from both inductive and capacitive coupling was theoretically analyzed by Lee and Chung,[29] who found that the pressure and the dimensions of the reactor affected the power for the E–H transition. The combined effects of electron density, collision frequency, and skin depth of the electromagnetic wave contribute to nonlinear dependence of the mode transition on operating conditions. The hysteresis of the E–H transition was experimentally investigated by Daltrini *et al.*[30] They suggest that rather than being an intrinsic characteristic of the plasma, the hysteresis behavior can be affected by the power loss in the matching system, suggesting the need to include circuit analysis when investigating these transitions.

The E-to-H transition is another complicating factor in matching pulsed power to the ICP reactor. The change in Z_L due to the E-to-H transition in addition to the reduction in the resistance of the plasma is typically over shorter times than the components in the match box can be changed. The end result is that power delivery cannot be efficiently matched to the plasma reactor during the entire pulsed cycle. The values of components in the match box are typically chosen to match at a particular time during the pulsed cycle—this is called set-point matching. If the match is chosen early in the pulsed period, the E-mode may be emphasized while there is a mismatch during the latter part of the pulsed cycle. If the set-point is late during the pulse period, the E-mode may be suppressed, but there is also a longer time to ramp up the plasma density when power is mismatched early in the pulse.

In this paper, we discuss results from a computational investigation of the dynamics of power matching to pulsed ICPs of the type used in microelectronics processing (etching and deposition). A model for the circuit and match box has been employed in a reactor scale two-dimensional model for the ICP. It was found that under perfect matching conditions, there is a smooth transition between the E- and H-modes, in contrast to several experimental results. This suggests that a sharp transition between modes is not a fundamental plasma transport issue but rather may be related to power delivery. It was found that when using pulsed power, the power delivery is highly dependent on the time during the pulse chosen for the set-point. Matching early in the pulsed period leads to a faster re-ignition of the plasma while emphasizing E-mode characteristics during the onset of the pulse. There is also poor matching during the H-mode. Matching later in the pulsed period leads to better power delivery overall at the cost of longer ignition delay. The rapid application of power when operating in the E-mode can launch electrostatic waves due to the need to establish a sheath to dissipate the applied voltage. The pulsed duty cycle, match box parameters, and antenna shape play key roles in power matching inductively coupled plasmas.

The model used in this investigation is described in Sec. II. Matching to pulsed ICPs with E–H transitions is discussed in Sec. III. Concluding remarks are in Sec. IV.

II. DESCRIPTION OF THE MODEL

This computational investigation was performed using the Hybrid Plasma Equipment Model (HPEM) complemented by a model for the match box. The HPEM is discussed in detail in Ref. 31, and so only a brief description will be provided here, including the unique aspects of the circuit calculation. The HPEM consists of modules that address different classes of physical phenomena and exchange information. In this case, we utilized three modules—the Electromagnetics Module (EMM), the Electron Energy Transport Module (EETM), and the Fluid-Kinetics Module (FKM). The frequency domain wave equation for the inductively coupled electric field is solved in the EMM. In this two-dimensional simulation, the current flowing in the antenna is in the azimuthal direction θ, producing components at the fundamental frequency of the magnetic field in the (r,z) (radius, height) directions and of the electric field, E_θ, in the θ direction. The conduction currents through each turn of the antenna that are used in the solution of the wave equation are provided by a circuit model, which also provides the fundamental frequency voltages on each turn of the antenna used in the FKM for the solution of Poisson's equation. Continuity, momentum, and energy equations (a fluid representation) are solved in the FKM for all charged and neutral species coincident with the solution of Poisson's equation for the electrostatic potential, Φ. In this two-dimensional simulation, Φ is solved in the (r,z) plane, providing electrostatic field components E_r, E_z. Electron heating is provided by the harmonic inductively coupled fields E_θ from the EMM. All components of the electrostatic (E_r, E_z) and electromagnetic fields (B_r, B_z, E_θ) are used in the EETM to track the trajectory of secondary electrons from surfaces using Monte Carlo techniques. Complex conductivities are transferred back to the EMM to solve the wave equation. One sweep through the modules is called an iteration of the model.

The EMM contains a circuit model with which the power supply is interfaced to the plasma reactor. A schematic of the circuit representation of the match box, antenna, reactor, and plasma is in Fig. 1. The antenna is represented as a discretized transmission line in the circuit model. The physical inductance of the antenna is determined by its overall diameter, height, number of turns, and thickness of the wire. This inductance is divided into 100 discrete series segments, each of which also has an appropriate fraction of the total resistance of the antenna. Each segment n of the transmission line contains a series impedance, Z_{Sn}, consisting of resistance (R_{An}) and physical inductance (L_{An}) of the antenna. Z_{Sn} also contains transformed values of resistance and inductance from the plasma.[33] The transformed impedance of the

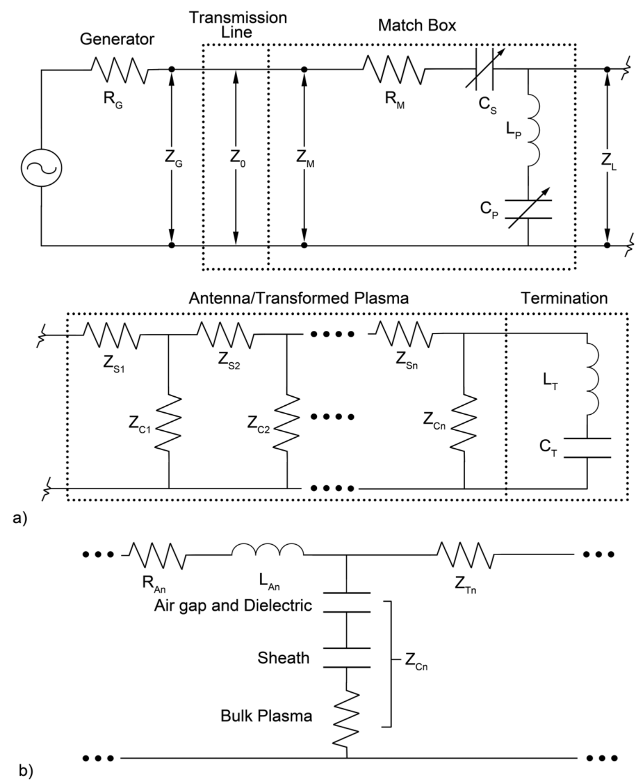

FIG. 1. Circuit schematic. (a) The circuit consists of impedances of the power generator, transmission line, matchbox, antenna, plasma, and termination circuit components. The antenna and transformed plasma impendances area represented by a discrete transmission line with each segment have having serial impedance Z_{Sn} and parallel impedance due to capacitive coupling Z_{Cn}. (b) The Z_{Sn} components consist of the physical resistance (R_{An}) and inductance (L_{An}) of the antenna, and the transformed impedance (resistance and inductance) of the plasma, Z_{Tn}. The impedance due to capacitive coupling, Z_{Cn}, has components due to the air gap and dielectric, sheath, and bulk resistance of the plasma.

plasma, Z_T, is[34]

$$Z_T = \left(\frac{\omega M}{Z_P}\right)^2 \left(-i\omega L_P + R_P\left(1 - i\frac{\omega}{\nu_m}\right)\right), \quad M^2 = k_A L_A L_P, \quad \text{(2a)}$$

$$Z_P^2 = \left(\omega L_P + \frac{\omega}{\nu_m} R_P\right)^2 + R_P, \quad \text{(2b)}$$

where ω is the radian frequency of the applied power, L_A is the physical inductance of the coil, L_P is the inductance of the plasma, ν_m is the electron momentum transfer collision frequency, R_P is the plasma resistance, and k_A is the antenna transformer coupling coefficient. The effective plasma resistance R_P is given by

$$R_P = \frac{\int \vec{j}_\theta \cdot \vec{E}_\theta \, d^3 r}{\left(\int \vec{j}_\theta \cdot d\vec{A}\right)}, \quad (3)$$

where the numerator is the volume integrated inductively coupled power and the denominator is the area integrated azimuthal current. The consequences of skin depth and nonlinearities in the plasma are accounted for by the spatial dependence and phase differences between the current and the electric field.

From each discrete segment of the transmission line representation of the antenna, a capacitance and series resistance is directed to ground, collectively represented by an impedance Z_{Cn}. The impedance Z_{Cn} represents the capacitive coupling from the antenna through the plasma to grounding. The reactance of Z_{Cn} consists dominantly of the series capacitances of the air gap between the antenna and the dielectric window of the ICP reactor, the window, and the plasma sheath at the surface of the window. The resistance of Z_{Cn} consists of the bulk plasma conducting capacitive current to ground. During execution of the FKM, the impedance of each element Z_{cn} is determined as follows.

For each turn k of the antenna, the voltage amplitude V_{ok} and phase ϕ_{vk} are determined from the circuit model. The voltage $V_k(t) = \mathrm{Re}(V_{ok}\exp(i(\omega t + \phi_{Vk}))) = V_{ok}\cos(\omega t + \phi_{Vk})$ is used as a boundary condition on the metal of the antenna for the solution of Poisson's equation in the FKM. Since the antenna is outside the plasma and not touching a conductive surface, the current flowing perpendicular to the surface of the antenna, that is the (r,z) components of current, is purely displacement current. The displacement current flowing out of each turn k of the antenna is computed as an integral over the surface of the antenna having normal $\hat{n}$,

$$I_k(t) = \int \varepsilon_k \frac{d(\vec{E}(t)\cdot\hat{n})}{dt} dA, \quad (4)$$

where E is the electrostatic electric field produced by the solution of Poisson's equation and ε_k is the permittivity of the material in contact with the antenna. The resulting current is then Fourier analyzed to provide the amplitude I_{ok} and the phase ϕ_{Ik} of the current at the fundamental frequency ω. $I_k(t) = \mathrm{Re}(I_{ok}\exp(i(\omega t + \phi_{Ik})))$.

The impedance Z_k is then given by

$$Z_k = \frac{V_{ok}}{I_{ok}} \exp(i(\phi_{Vk} - \phi_{Ik})). \quad (5)$$

The real part of Z_k represents the dissipative resistance (or capacitive power deposition). The imaginary part of Z_k is the reactance. For purely H-mode operation, $(\phi_{Vk} - \phi_{Ik})$ tends toward -90° resulting in negligible capacitive power deposition with Z_k being capacitively reactive (negative imaginary). With E-mode contributions, $-90^\circ < (\phi_{Vk} - \phi_{Ik}) < 0$, and there is a finite real resistive component. These values of Z_k are then distributed along the transmission line representing the antenna in the circuit model. That is, Z_{Cn} is then a fractional assignment of Z_k to those segments n of the antenna associated with turn k. In a similar way, the total capacitive power is the sum of the power dissipated by each turn of the antenna and is computed as a cycle average of

$$P_c = \sum_k P_k = \sum_k \frac{1}{\tau_{rf}} \iint \varepsilon_k V_k(t) \frac{d(\vec{E}(t)\cdot\hat{n})}{dt} dA dt. \quad (6)$$

The power delivered by the power supply is specified as a function of time. This power is delivered into a transmission line between the supply and the match box. Plasma conductivities, P_c and Z_k, are provided by the FKM. Using these values, the circuit equations representing the match box and plasma reactor are solved, which produces antenna currents that are then used in the solution of the wave equation to generate the amplitude $E_\theta(r,z)$ and phase $\phi(r,z)$ of the azimuthal electric field. The solution of the circuit equations also produces P_A (resistive losses in the antenna coils), P_M (resistive losses in the match box), and Z_M (the input impedance to the matchbox). The power dissipated by inductive coupling in the plasma is

$$P_I = \int \frac{1}{2} \sigma(\vec{r}) E_\theta^2(\vec{r}) d^3 r. \quad (7)$$

For the purposes of this study, we assumed that inductive power deposition in the plasma is collisional while acknowledging that at low pressures of interest, power deposition has non-local components. The methods described here are completely general and apply to the case of non-collisional heating where kinetic methods are used to derive P_I.

With Z_M, we compute the reflection coefficient, Γ, for power delivered by the supply, P_S,

$$\Gamma = \frac{Z_M - Z_0}{Z_M + Z_0}. \quad (8)$$

We ignored the consequences of the reflected power back to the power supply. In a fully self-consistent solution, we should have the total power dissipation in the system, P_T, as

$$P_T = (1 - \Gamma) P_S = P_M + P_A + P_I + P_C, \quad (9)$$

where P_A is the resistive power dissipated in the antenna and P_M is the resistive power dissipated in the match box. This equality is typically not obtained. Recognizing that E_θ scales linearly with the antenna current and P_I scales with E_θ^2, the current flowing into the match box is renormalized so that the equality for P_T is obtained. With these renormalized values, the circuit and wave equations are again solved. The process is iterated several thousand times to convergence. At the end of this process, the final values of V_k, E_ϕ, and θ are returned to the FKM and EMM for the next iteration through the modules for time integration of the fluid equations for densities, momenta, and energy, typically for a duration of 100s of ns to 0.5 μs. During this time, amplitudes V_k and E_ϕ, and the phase θ are not changed.

For a perfect match of P_S to the plasma reactor, we must have $Z_M = Z_0$. For this architecture of the circuit, matching is produced by adjusting C_P and C_S such that $\mathrm{Re}(Z_M) = Z_0$ and $\mathrm{Im}(Z_M) = 0$. From a procedural perspective, these values can be searched for by varying C_P and C_S to minimize the value of Γ. For select circuit architectures, one can analytically compute Z_M based on the circuit values and solve for the values of C_P and C_S that produce the match ($Z_M = Z_0$). The method of the solution for C_P and C_S, called the perfect match values, appears in the Appendix.

III. MATCHING TO PULSED ICPs WITH E–H TRANSITIONS

For computationally investigating the fundamental phenomena of E–H matching, we chose a simple ICP geometry and a relatively small chamber. This layout for an ICP reactor powered by a spiral planar antenna is a standard design used for plasma assisted semiconductor fabrication.[35–37] Industrial systems are typically larger to accommodate wafers up to 30 cm in diameter. Our choice of a smaller chamber for this investigation was based on wanting a fine enough mesh to capture the dynamics of the E–H transitions while also enabling computation of a sufficient number of pulsed periods to reach the quasi-steady states. The details of our investigation are sensitive to the size and topology of the reactor. For example, antenna and chamber impedance are both functions of size and layout, which would affect the specific values of match box parameters and necessitate a different termination impedance. The spacing of the antenna from the dielectric window affects capacitive coupling, as discussed below. Having said that, the systematic trends we discuss apply to more complex and larger reactors. For example, we have performed limited studies on industrial size ICP reactors,[38] and the systematic trends we discuss here are essentially the same.

A schematic of the reactor is shown in Fig. 2. The chamber has an internal diameter of 22.5 cm, has a height (substrate to window) of 12 cm, and is powered by a three-turn antenna having radii of 2.5, 5.3, and 8.0 cm. The coils have a thickness of 0.45 cm and a height of 1.15 cm and sit above the 0.8 cm thick quartz window ($\varepsilon/\varepsilon_0 = 4$) with an air gap of 0.4 cm. The total inductance of the antenna is $L_C = 0.95\,\mu$H. The antenna–plasma coupling coefficient is $k_C = 0.75$. The entire inner surface of the window serves as a gas inlet showerhead with the pump port occupying an annulus between 6.9 and 11.1 cm on the bottom of the chamber. A pressure sensor is located in the outer wall 2 cm above the pump port. All other surfaces are grounded metal.

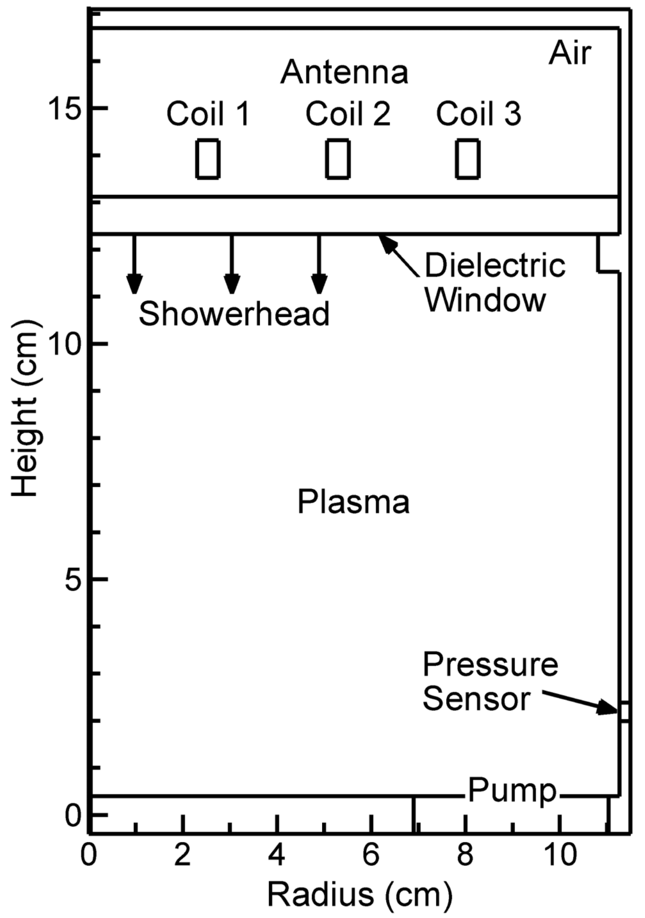

FIG. 2. Geometry of the cylindrically symmetric ICP reactor.

Unless otherwise noted, the gas mixture is Ar/Cl_2 = 65/35 at a pressure of 25 mTorr. Ar/Cl_2 gas mixtures are commonly used for conductor etching. The gas inlet flow rate is 200 sccm. The outlet flow rate is adjusted so that the pressure at the sensor is 25 mTorr. As discussed below, our results are sensitive to the conductivity of the plasma at the start of the power pulse and that conductivity is sensitive to the gas mixture. When using pure Cl_2 plasmas, a thermal electron attaching gas, the system can transition to an ion–ion plasma during the afterglow with a negligible electron density. These conditions then require "re-ignition" of the plasma on every power pulse. Although this may in fact be the case for many industrial systems, the re-ignition requirement adds another constraint and complexity. We, therefore, chose a gas mixture for which there would be a significant change in conductivity during the afterglow but not to the degree that re-ignition is required.

The reaction mechanism is the same as discussed in Ref. 32. An important point for this study is that Cl_2 is a thermal electron attaching gas for which the rate coefficient for dissociative electron attachment increases with decreasing electron temperature, T_e.

So for otherwise the same conditions, the rates of attachment are small when power is applied during a pulse and T_e is large. The rates of attachment are large when the power is off and T_e is small.

The fixed circuit elements are coil resistance $R_C = 0.1\,\Omega$ and termination impedances $C_T = 100\,\text{nF}$ and $L_T = 5\,\text{nH}$, and inductance in the match box $L_P = 100\,\text{nH}$. The internal resistance of the match box was neglected by setting $R_M = 10^{-6}\,\Omega$ so that P_M is small. This allows for the independent study of impedance matching impact on plasma transients. In practice, matching network impedances can have 100s to 1000s of mΩ of real resistance and consume a significant amount of power delivered by the supply. Typically, these dissipative losses are accounted for in the series elements, where the larger dissipative components tend to reside and where the current through the elements tends to be higher, as opposed to the shunt components. The inner coil of the antenna was connected to the match box, and the outer coil of the antenna was connected to grounding through the series termination components C_T and L_T.

A. Continuous power baseline

With the base case values for circuit and operating conditions, the continuous wave (CW) characteristics of the ICP reactor were first investigated as a function of power delivered from the supply. Using perfect match values for C_P and C_S (see the Appendix), $\Gamma = 0$ and $P_S = P_T$. The electron density, inductive power, and capacitive power are shown in Fig. 3 for a total power deposition of 5 W and 200 W. Note that the capacitive power deposition plotted is actually the time average of the capacitive and resistive (bulk) power deposition. The calculation of local power deposition of $p = \vec{j} \cdot \vec{E}$ is unable to distinguish between the capacitive and resistive heating. Given the spatial distribution and the negative sign of the reactance of Z_k, the capacitive power is clearly dominated by sheath heating at a higher total power.

For 5 W, the voltages on the coils (inner to outer) are 147 V, 112 V, and 44 V. The total capacitive power is 3.19 W (63.8% of the total), inductive power is 0.86 W (17.2%), and resistive antenna losses are 0.95 W (19%), a power division that indicates the E-mode operation. On a relative basis, antenna losses are larger at a lower total power due to the higher relative antenna current required to sustain the plasma. The capacitive component includes contributions from both ion and electron acceleration by the sheath and bulk Joule heating. With the largest voltage and capacitive current from the inner coil, the capacitive heating is maximum under that coil (3.8 mW/cm^3) adjacent to the dielectric with resistive current flowing through the plasma to produce Joule heating of 0.7 mW/cm^3 in the center of the plasma. Sheath heating also occurs along the metal boundaries. With the peak electron density of $6 \times 10^8\,\text{cm}^{-3}$, inductive power deposition extends to the middle of the reactor (electric field skin depth $\lambda_E = 7.4\,\text{cm}$) with a maximum value of 3 mW/cm^3. The voltages on the three coils of the antenna are nearly in phase. However, with different voltage amplitudes and different adjacent sheath thicknesses, particularly with respect to ground, there is some recirculation of current between the antenna coils that produce a net negative power deposition in the upper outer radius of the reactor.

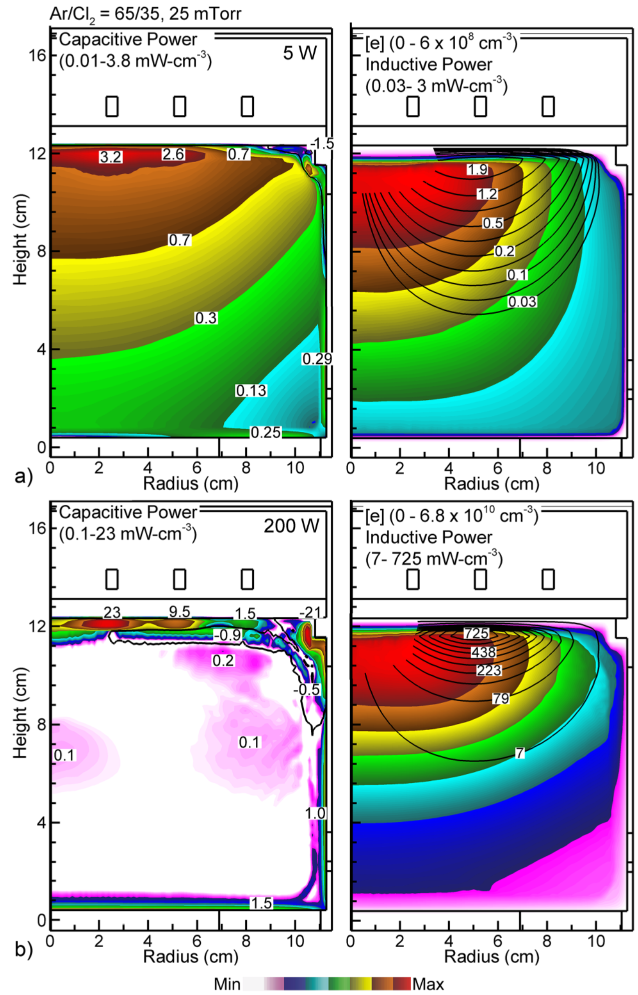

FIG. 3. Capacitive and inductive power deposition, and electron density when plasma is sustained with at a total continuous power of (a) 5 W and (b) 200 W (Ar/Cl$_2$ = 65/35, 25 mTorr). The match is perfect. The capacitive power and is shown as color contours with a line separating the positive and negative values. Contour labels are mW/cm^3. Electron density is shown as color contours. Inductive power deposition is shown as contour lines with labels in mW/cm^3. The contour lines are blanked near the axis to enable a clear view of the sheath formed under the powered coil.

For 200 W total power, the voltages on the coils (inner to outer) are 334 V, 276 V, and 112 V. The total capacitive power is 9.7 W (4.8% of the total), inductive power is 188.2 W (94.1%), and resistive antenna losses are 2.1 W (1.1%), a power division that indicates the H-mode. With a higher electron density (peak $6.8 \times 10^{10}\,\text{cm}^{-3}$), the plasma is more conductive and capacitive heating is largely limited to the periphery of the reactor. The higher plasma density also reduces the electric field skin depth to $\lambda_E = 0.7\,\text{cm}$.

The capacitive power has a cycled averaged layer of negative power deposition parallel to the dielectric window, in addition to that in the upper right corner, which was not observed at lower power. At high power, the electron flux directed toward the dielectric is dominated by the ambipolar flux originating from the electron sources produced by inductive coupling. The electron ambipolar flux is retarded by the ambipolar electric field that points from the center of the plasma toward boundaries. This is the same direction as the electric field that produces electron heating due to the expansion of the capacitive sheath under the window. During the expansion of the capacitive sheath, power is expended in slowing the ambipolar driven electron flux in addition to accelerating electrons out of the sheath region. This negative power deposition is not observed at the lower power in the absence of the large ambipolar electron flux produced by inductive coupling.

The division of power deposition between capacitive and inductive coupling and average electron density are shown in Fig. 4(a) for $P_T = 5$–200 W for perfect match conditions and continuous power. The values of C_P and C_S to obtain perfect matches and ionization efficiency are shown in Fig. 4(b). (Ionization efficiency is average plasma density divided by power deposition in the plasma and is a relative measure of efficiency.) These results are typical of the E–H transition. At low power deposition, the electron density is low, the skin depth is large, and the sheath is thick. The low electron density and large skin depth reduce (on a relative basis) the inductive power deposition, and the thick sheath (on a relative basis) increases the capacitive power deposition. The thicker sheaths produce a larger sheath velocity, and capacitive power deposition scales with the square of the sheath speed. As noted above, for $P_T = 5$ W, 77% of the power is capacitive and 11% is inductive. The power dissipation by the coil is about 12%. With increasing power deposition, the electron density increases, skin depth decreases, and sheath thickness shrinks, all of which contribute to lower capacitive power deposition and higher inductive power deposition. We do not observe a sharp, step-function increase in electron density that can be identified as the E–H transition. The power at which the E–H transition occurs is then somewhat a qualitative judgment. The fraction of power dissipated by inductive coupling exceeds 50% at $P_T = 25$ W and exceeds 90% at $P_T = 140$ W. To achieve the perfect match, the values of the matching elements C_P decrease by about 20% and C_S increase by a factor of 2.5.

Over the range of $P_T = 5$–200 W, the average electron density increases from 2.8×10^8 cm^{-3} to 2.3×10^{10} cm^{-3}, an increase by a factor of nearly 100, for P_T increasing by a factor of 40. A portion of the increase in electron density results from an increase in ionization efficiency, plotted here as the total electron density divided by the total power deposition in the plasma. This efficiency increases by a factor of nearly 3. At low P_T, the fraction of power dissipated by the resistive coil and capacitive heating is large. No ionization occurs from coil heating, and the efficiency of ionization by capacitive coupling is low due to ion acceleration in the sheaths, characteristic of the E-mode. The efficiency remains relatively constant until the H-mode begins, at which time the efficiency increases. At high power deposition, a true H-mode occurs, as the majority of power is dissipated by electron heating in the bulk, which is intrinsically more efficient at producing ionization.

With there always being a perfect match when changing P_S, there is a relatively smooth transition from the dominant E-mode to the dominant H-mode with increasing power. To obtain this perfect match with increasing power, the value of C_S smoothly increases (from 33 pF to 155 pF) and C_P smoothly decreases (from 267 pF to 168 pF). Experimentally, it is often observed that there is a rapid, almost impulsive, increase in electron density with a rapid switch between the E-mode and the H-mode when a critical power is delivered from the supply. Based on fundamental plasma transport, there is no requirement for such a sharp transition to occur.

In practice, the transition in apparent ionization efficiency may be exacerbated by the difficulty in matching between the E-mode and the H-mode. If the circuit is better able to match to the H-mode (positive reactance) than the E-mode (negative reactance), then the ionization efficiency will make a rapid and

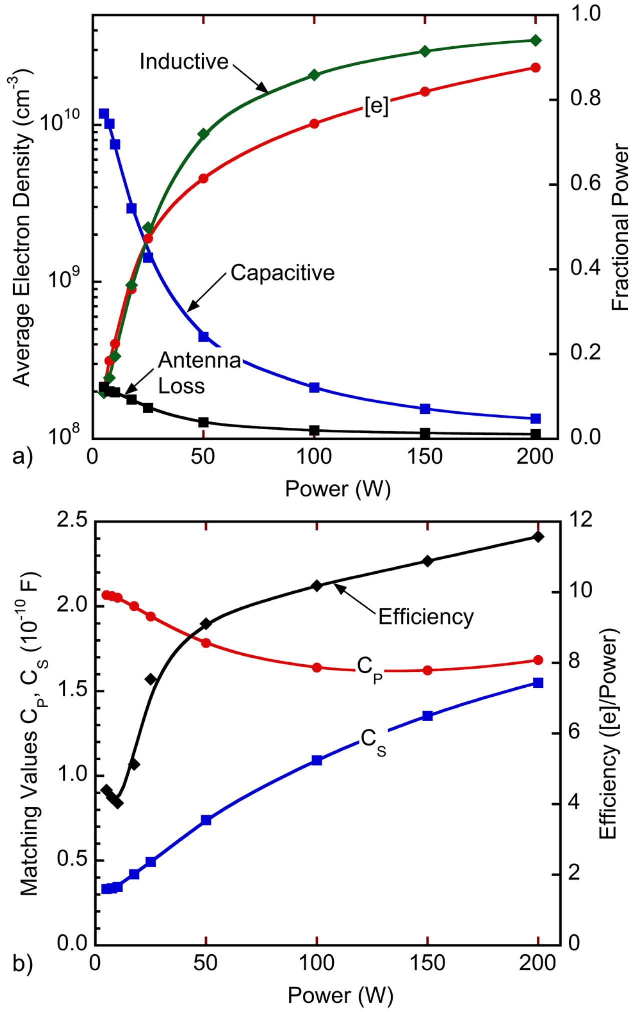

FIG. 4. Plasma and circuit properties as a function of CW power deposition for perfect matching (Ar/Cl_2 = 65/35, 25 mTorr). (a) Electron density and fraction of power deposition due to the inductive H-mode, capacitive E-mode, and antenna heating. (b) Analytical solutions for C_P and C_S for a perfect match and the ionization efficiency. The ionization efficiency is total electron density divided by power deposition in the plasma and is a relative measure of efficiency.

impulsive increase when the H-mode begins to dominate. There may also be heating of electrical components that can change their impedance. Another factor that may influence the apparent ionization efficiency is changes in plasma conditions due to the power deposition. For example, when operating at a constant pressure, higher power deposition produces more gas heating that reduces the gas density and so reduces the electron collision frequency. In chemically active mixtures, more power deposition produces more dissociation and so there are different species with which electrons collide.

To demonstrate these possibilities, two parameterizations were performed. In the first, a parameterization over power (P_T = 5–200 W) was conducted with the match box settings chosen to provide a perfect match at 150 W (C_P = 162 pF and C_S = 135 pF), which then produces mismatches at other powers. The resulting ionization efficiency is shown in Fig. 5. For these conditions, the circuit is mismatched at lower powers, producing a large reflection coefficient and a corresponding low ionization efficiency. With power increasing toward 150 W, the reflection coefficient decreases, the H-mode begins to dominate, and so the ionization efficiency increases.

In the results shown in Fig. 4, the length of time for the simulation was deliberately chosen to be long enough so that the plasma properties came into a quasi-steady state; while being short enough so that there was no significant dissociation of the feedstock gases and gas temperature excursions were not significantly different. These conditions correspond to a short residence time of the gas in the plasma, τ_{res}. In this way, a side-by-side comparison of different powers could be performed without the complication of the impact of changing gas temperatures, gas densities, and gas compositions on matching. In actual practice, when changing power, one does have these complications of gas heating producing rarefaction and different degrees of dissociation of the gas.

The parameterization in Fig. 4 was repeated when computing for a sufficient time that all plasma properties including gas temperature and composition come into a steady state. This would correspond to at large τ_{res}. With large τ_{res}, for P_T = 5 W, the average gas temperature was T_g = 330 K (for a wall temperature of 325 K) and fractional dissociation of Cl_2 was 1.3%. For P_T = 200 W, T_g = 635 K and fractional dissociation was 27%. The resulting ionization efficiency, also shown in Fig. 5, increases by a factor of 4.5 from low to high power. The majority of this increase in efficiency results from the decrease in Cl_2 mole fraction (due to dissociation) and decrease in gas density (gas heating), which then decreases the rate of attachment. These results emphasize the difficulty of performing side-by-side comparisons of the E–H behavior when changes in power deposition also change the fundamental properties of the plasma in addition to electron density.

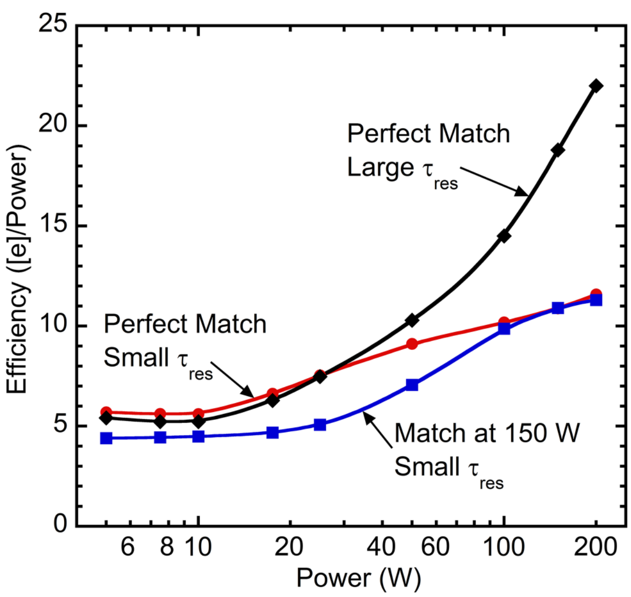

FIG. 5. Ionization efficiency as a function of CW power (Ar/Cl_2 = 65/35, 25 mTorr). Cases are shown for perfect matches for small and large residence time (τ_{res}) and with circuit values for a perfect match at 150 W with small τ_{res}. The ionization efficiency is the total electron density divided by power deposition in the plasma and is a relative measure of efficiency.

B. Set-point matching to pulsed ICPs

In this section, we discuss matching of a pulsed ICP for the same operating conditions as the CW studies (Ar/Cl_2 = 65/35, 25 mTorr). The standard conditions for pulsed ICP operation were a pulse repetition rate (PRF) of 13.3 kHz (period of 75 μs), a duty cycle of 35%, and forward power delivered from the supply during the power-on period of P_S = 250 W. As a base case, we used perfect match conditions by instantly adjusting C_P and C_S to produce $\Gamma = 0$ throughout the pulse period. The maximum in the plasma potential, the electron density, Cl^- density, and positive ion densities are shown in Fig. 6(a) during the power pulse and immediate afterglow. The modes of power dissipation are shown in Fig. 6(b). The resistive and reactive components of the impedance Z_L and perfect matching values of C_P and C_S are shown in Fig. 6(c).

At the beginning of the power pulse, the plasma conditions are essentially an ion–ion plasma where the positive ion density is nearly equal to the negative ion density, $[M^+] \approx [Cl^-] = 4.5 \times 10^{10}\ cm^{-3}$. The small electron density at the beginning of the pulse, $n_e = 2 \times 10^8\ cm^{-3}$, results from Cl_2 being a thermally attaching gas, which reduces the electron density during the afterglow through the dissociative electron attachment producing Cl^-. During the power pulse, the negative ion density $[Cl^-]$ is relatively constant. With the electron temperature $T_e \approx$ 2.5–3.5 eV during the power pulse, the thermal dissociative attachment rates are small compared to ionization rates. The increase in electron density is nearly matched by the increase in positive ion density.

With this low initial electron density, power is initially capacitively coupled. During the first 3 μs, the capacitive power exceeds that of the inductive power and the plasma operates in the E-mode. The E-mode is additionally indicated by the oscillation in the plasma potential, Φ_P, with an amplitude as large as 450 V in the same manner as a capacitively coupled plasma. The maximum antenna voltage amplitude (inner turn) is 1080 V. There is some oscillation in the voltage amplitude on the antenna, which is due to the rapid increase in electron density, which changes the plasma

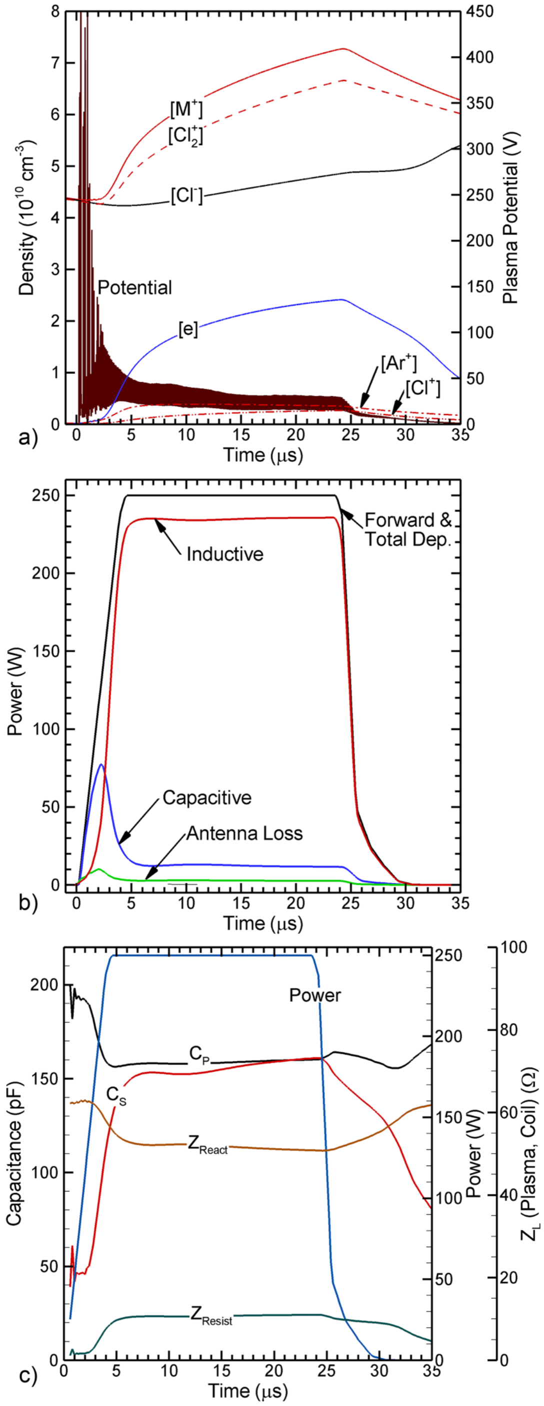

FIG. 6. Plasma and circuit values for a pulsed ICP with perfect matching. (a) Electron and ion densities and plasma potential, (b) modes of power deposition, and (c) C_P and C_S for perfect match conditions and reactive and resistive components of the impedance Z_L. The pulse repetition frequency is 13.3 kHz, duty cycle of 35%, and forward power during the pulse is $P_S = 250$ W, shown in (c).

impedance sufficiently to lower the antenna voltage and lowers the electron density that induces an increase in antenna voltage. This oscillation is likely magnified by the iterative numerical technique used to link the plasma portion of the simulation with the circuit.

As the electron density increases, the electromagnetic skin depth decreases, the sheath under the coils thins, and the fraction of capacitive power dissipation decreases. By 5 μs, the electron density is high enough, 1×10^{10} cm^{-3}, and the skin depth is short enough so that power is dominantly inductively coupled and the plasma operates dominantly in the H-mode. Due to the proximity of the antenna to the dielectric window, approximately 5% of the total power continues to be capacitively coupled even during the H-mode. This is similar to the CW operation. In the quasi-steady state during the pulse, the proportion of capacitively coupled power decreases by a few watts but is otherwise nearly constant. Upon termination of the power, both the capacitive and inductive powers decrease in nearly the same proportion while remaining in the H-mode. The power decreases quickly enough so that the electron density does not appreciably change, and the skin depth remains short enough to allow the H-mode operation. This represents a hysteresis-type of behavior. The plasma remains in the H-mode during decreasing power at the same power deposition that corresponded to the E-mode during the beginning of the pulse.

As the plasma density increases at the leading edge of the power pulse and operation transitions to the H-mode, the oscillation in Φ_P decreases to an amplitude of 10–20 V. This modulation of Φ_P is on top of the quasi-dc plasma potential of about 20 V. This dc value of plasma potential results from the ambipolar nature of the plasma transport ($T_e > T_{\rm ion}$, $m_e < m_{\rm ion}$). An indication of purely H-mode operation without capacitive coupling would be quasi-dc plasma potential without significant oscillation. Since the power deposition resulting from E_θ and electron heating are harmonic, there can be harmonic oscillation in T_e, and so there would be some small oscillation in Φ_P even in the pure H-mode. However, in this case, the majority of oscillation in Φ_P is due to capacitive coupling.

With perfect match conditions, C_P decreases during the power pulse from 290 pF to 160 pF, accompanied by an increase in C_S from 50 pF to 160 pF. The combined load impedance, Z_L (which includes the antenna coil and plasma) has a positive reactance due to the inductance of the antenna. This reactance decreases during the plasma pulse in response to the capacitive component of the antenna current through the plasma. The resistive component increases in response to power deposition in the plasma.

The impedance of the variable capacitors in the RF matching network is typically changed by a mechanical process (e.g., changing the overlap area between two plates). The speed of the mechanical movement of these variable capacitor systems is largely determined by the driving motors, with end-to-end movement typically on the order of hundreds to thousands of milliseconds. Impedance control algorithms working in conjunction with these mechanical limits will typically produce a tuning transient with a comparable characteristic time. With plasma-induced impedance transients having time scales that are orders of magnitude shorter that what can be achieved by these mechanically driven systems, it is typically not possible to change the values of C_S and C_P rapidly enough to achieve a perfect match throughout the power pulse.

Typically, set-point matching is employed in which values of C_S and C_P are chosen to minimize Γ at a particular instant during the power pulse. We investigated the consequences of set-point matching. Computationally, this was achieved by selecting values at given times for C_S and C_P from the perfect match case. For example, the plasma reactor properties are shown in Fig. 7 when values for C_S and C_P were chosen for set-point matches from early to late in the pulse. These times, relative to the start of the power pulse, were 1.5, 3.25, 7, and 21 μs. Since the progression of the plasma prior to the time of the matching point is not exactly the same as for the case with perfect matching, the reflection coefficient at the match point may not be exactly zero.

For a matching point of $t_M = 1.5\,\mu$s, the reactor properties at the match point are a forward power of 82.7 W and $\Gamma = 0.013$. The maximum capacitive power of 62.2 W occurs at the match point. The resistive power is 9.6 W and inductive power is 8.5 W, indicating operation in the E-mode. (Note that Γ is finite due to the plasma properties being different than for the perfect match that provided the values of C_S and C_P.) As the plasma density begins to increase, the E-mode dissipates and the H-mode begins. With this increase in plasma density, the values of C_S and C_P required to achieve a match deviate from the set-point values. The reflection coefficient then monotonically increases until the H-mode is fully established at $t = 6$–$7\,\mu$s, after which Γ is relatively constant at 0.5. At the end of the pulse, the electron density is $1.15 \times 10^{10}\,\mathrm{cm}^{-3}$ compared to the perfect match value of $2.4 \times 10^{10}\,\mathrm{cm}^{-3}$. This decrease in electron density is due to the reduction in power deposition following that $\Gamma = 0.5$.

As t_M increases, the peak capacitive power decreases, there is a larger delay in the onset of inductive power deposition and the maximum inductive power increases, as shown in Fig. 8. The delay in the onset of the H-mode results from there being less ionization produced during the E-mode. With a larger t_M, there is a larger mismatch that produces a larger Γ early in the pulse, which reduces power deposition and ionization. For example, for $t_M = 2.5\,\mu$s, the peak capacitive power of $P_C = 70$ W occurs at $2\,\mu$s when the inductive power is $P_I = 41$ W and $\Gamma = 0.03$. Just prior to the end of the maximum delivered power at $23\,\mu$s, $P_C = 9.3$ W, $P_I = 108$, and $\Gamma = 0.46$. For $t_M = 21\,\mu$s, the peak capacitive power of $P_C = 21$ W occurs at $2.6\,\mu$s when the inductive power is $P_I < 1$ W

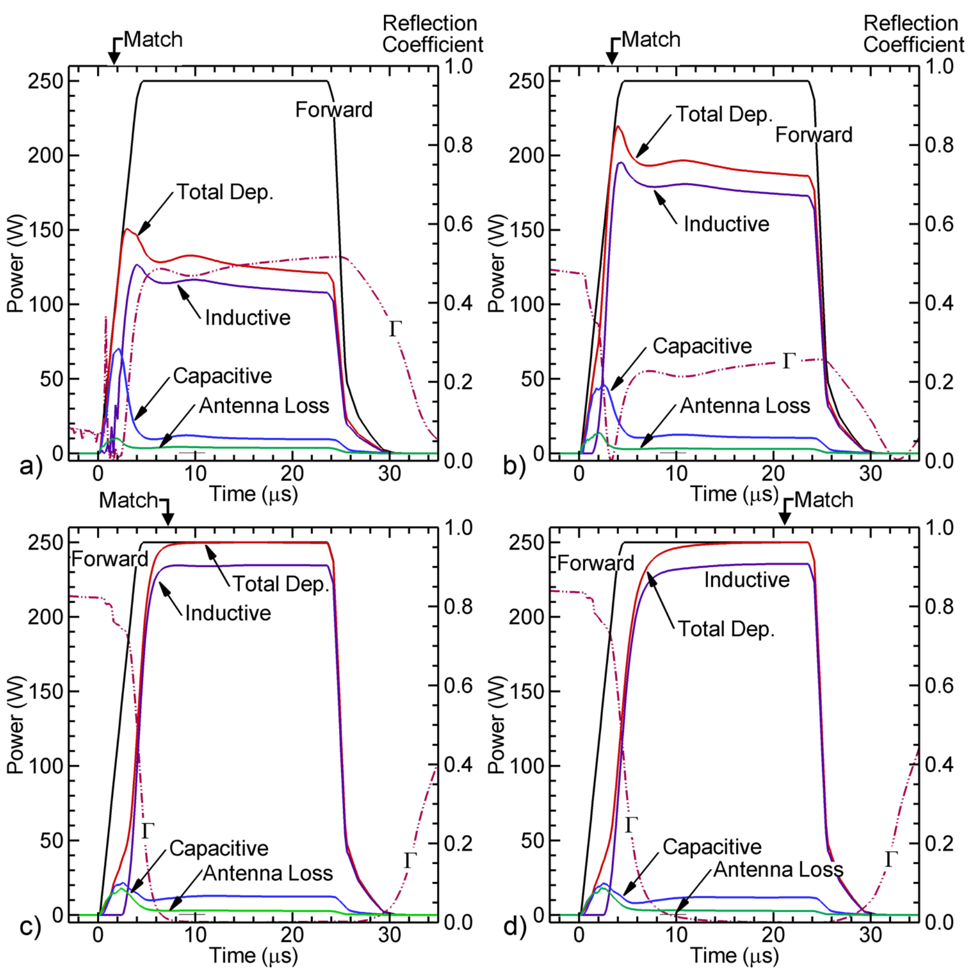

FIG. 7. Modes of power deposition, total power deposition, and power reflection coefficient Γ when C_P and C_S are chosen to match at t_M = (a) 1.5, (b) 3.25, (c) 7, and (d) 21 μs into the pulse (Ar/Cl_2 = 65/35, 25 mTorr, PRF = 13.3 kHz, DC = 35%, P_S = 250 W).

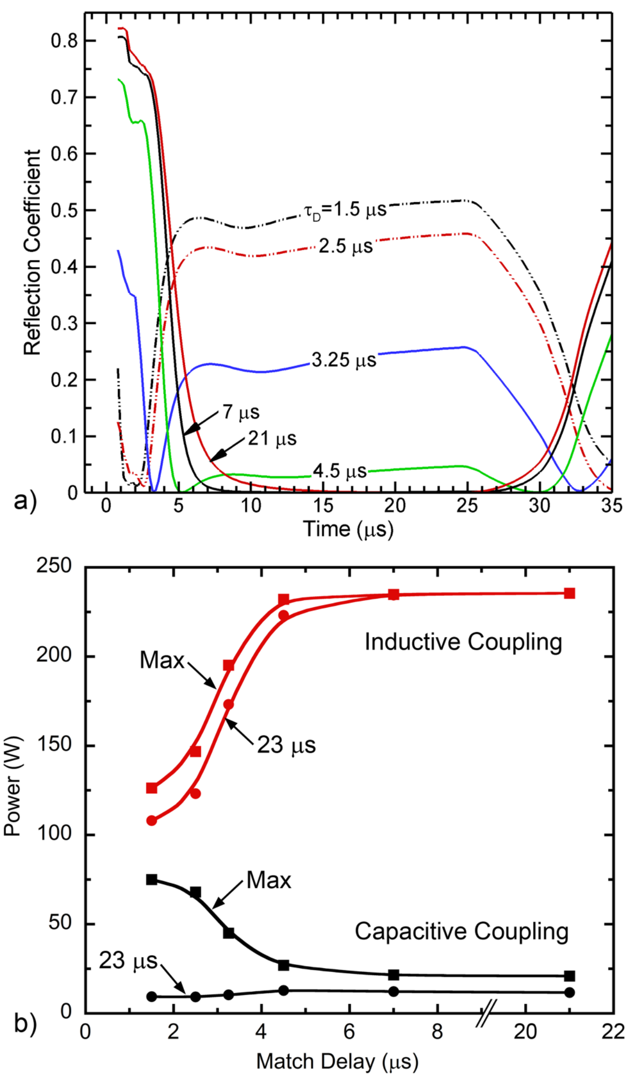

FIG. 8. Circuit values and power deposition as a function of matching time. (a) Power reflection coefficients through one pulsed period when matching at different t_M. (b) Inductive and capacitive power at their maximum value and at the end of pulse ($t = 23\,\mu s$) with varying match time t_M ($Ar/Cl_2 = 65/35$, 25 mTorr, PRF = 13.3 kHz, DC = 35%, $P_S = 250$ W).

and $\Gamma = 0.76$. At $23\,\mu s$, $P_C = 12$ W, $P_I = 235$, and $\Gamma < 0.001$. For $t_M > 7\,\mu s$, the set-point values of C_S and C_P are well matched to the H-mode, and so $\Gamma < 0.01$ for $t > 10$–$15\,\mu s$ for the remainder of the power pulse. The electron density at the end of the power pulse is nearly that of the perfect match.

C. Matching for different duty cycles

Matching early during the power pulse is sensitive to the electron density at the onset of power, and this is particularly problematic in thermally attaching gas mixtures such as Ar/Cl_2. During the inter-pulse period, the electron temperature decreases, which increases the rate of attachment and increases the electron loss. The lower electron density at the onset of power for the next pulse makes the system appear to be more capacitive to the matching network. This sensitivity can be demonstrated by varying the duty cycle of the pulsed power.

For the same peak power during the power pulse, a shorter duty cycle translates to lower average power deposition and less fractional dissociation of Cl_2. The larger density of Cl_2 results in more attachment during a longer inter-pulse period, resulting in a lower initial electron density at the beginning of the next pulse. For example, the electron density and plasma potential Φ_P during the pulsed period are shown in Fig. 9 for different duty cycles (25%–65%). Note that the time scales are shifted in Fig. 9(b) by increments of $10\,\mu s$ in order to show the plasma potentials more clearly. The electron density at the beginning of the pulsed cycle is $1 \times 10^8\,cm^{-3}$ for a duty cycle of 25% and $1 \times 10^9\,cm^{-3}$ for a duty cycle of 65%. The magnitude of oscillation of Φ_P indicates the severity of capacitive coupling.

When varying the duty cycle, the same set-point match is used corresponding to $t_M = 7\,\mu s$ and a duty cycle of 35%. Duty cycles shorter than 35% produce smaller initial electron densities. However, the system already starts in the E-mode, and so there is little change in the oscillation of Φ_P. Increasing the duty cycle increases the initial electron density, which enables some H-mode coupling early during the pulse. This H-mode coupled power reduces the power coupled into the E-mode, which then reduces the oscillation in Φ_P. This reduction in capacitive power does come at a cost of increasing the reflection coefficient. At the time of the nominal match conditions for a duty cycle of 35%, the reflection coefficient at $t = 7\,\mu s$ is $\Gamma = 0.01$. For a 25% duty cycle, $\Gamma = 0.02$ (still small), whereas for a duty cycle of 65%, the reflection coefficient is $\Gamma = 0.08$.

D. Ion energy distributions (IEDs) onto the window during the E-mode

A consequence of early matches that allow significant power into the E-mode is large ion fluxes incident onto the dielectric window while there is still significant oscillation in the plasma potential. These conditions produce energetic ions onto the window, which can result in sputtering and erosion. For example, ion energy distributions (IEDs) incident onto the window with a duty cycle of 25% are shown in Fig. 10. At the beginning of the pulse, the plasma potential rises from about 10 V when the sheath beneath the window is thick. The resulting IED is largely thermal with an extended tail. As the plasma density increases, which thins the sheath, and plasma potential increases with the capacitive coupling, the IED extends to as high as 200 eV, for a plasma potential peaking at 375 V during the E-mode. The maximum in the IED does not directly correspond to the maximum in plasma potential due to the locations within the thick sheath that ions are produced and due to the transient charging of the dielectric. As the H-mode is established and the plasma potential decreases, the maximum energy of the IEDs also begins to decrease. By the end of the power pulse, the peak of the IED occurs at 18 eV. In the afterglow where the plasma potential decreases below 10 V, the peak in the IED occurs at 5 eV.

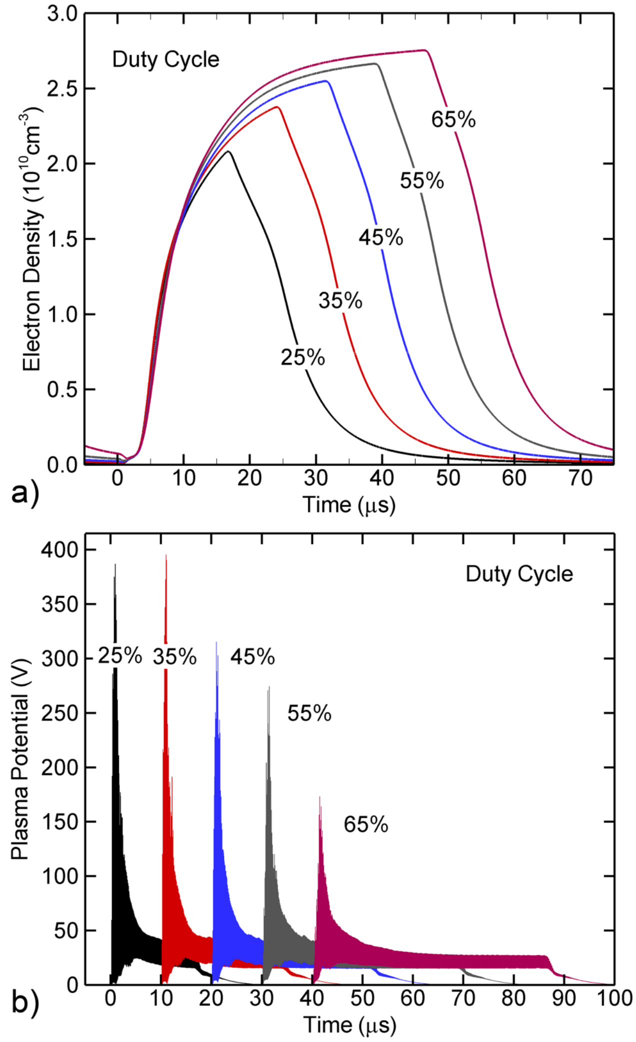

FIG. 9. Plasma properties when varying duty cycle (25%–65%) during a pulsed period. The circuit match values correspond to a duty cycle of 35% with the match time at $t_M = 7\,\mu$s. (a) Electron density and (b) plasma potential. For clarity, the plots for plasma potential have been shifted by increments of 10 μs (Ar/Cl_2 = 65/35, 25 mTorr, PRF = 13.3 kHz, P_S = 250 W).

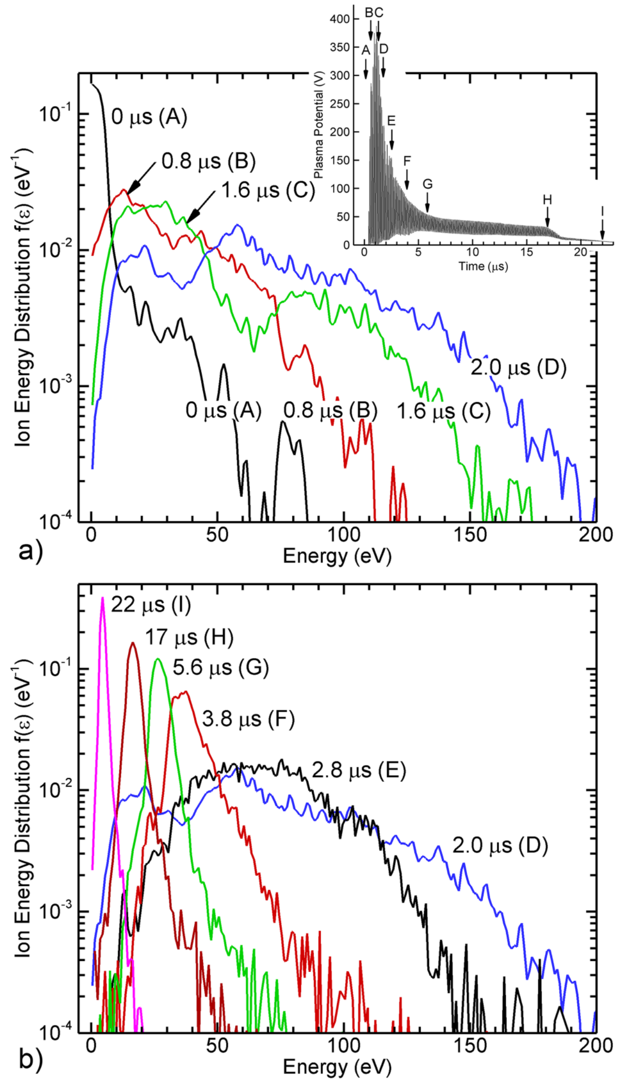

FIG. 10. Ion energy distribution (IED) incident onto the dielectric window at different times during the pulse. (a) 0–2.0 μs and (b) 2.0 μs–22 μs. The inset shows the plasma potential. The labels A–H are the locations in the pulsed cycle at which the IEDs are plotted. (Ar/Cl_2 = 65/35, 25 mTorr, PRF = 13.3 kHz, DC = 25%).

When matching early in the pulse, capacitive coupling is emphasized, there is more power dissipated in ion acceleration, and there are more energetic of ions incident on all inside surfaces of the reactor, and on the window, in particular. These energetic ions could be potentially damaging to the window and other surfaces. These energetic fluxes are then another consideration in choosing an early match. Having said that, even with t_M being small, the E-mode dissipates before the plasma density reaches its maximum value. As such, the flux of energetic ions produced by capacitive coupling may not be large, thereby reducing the likelihood for damage.

E. Antenna placement

The capacitance between the antenna and the plasma consists of at least three series components—the capacitance of the air gap between the antenna and window, the capacitance of the window, and the capacitance of the sheath. In practice, the capacitance of the antenna–window gap is more variable than that of the window. For example, placement of the antenna after maintenance must be extremely precise to replicate the capacitance of the antenna–window gap. The variable capacitance of the antenna–window gap then translates into variability in the plasma.

To demonstrate the sensitivity of matching pulsed ICPs to the placement of the antenna, the following procedure was followed. The gap between the bottom of the flat antenna and the window was varied from $d = 0$ (in contact with the window) to 8.2 mm. For each gap, calculations were first performed with perfect matching. The values of C_P and C_S for each gap size were then chosen as the perfect match values at $t_M = 20\,\mu$s. The simulations for gaps sizes of $d = 0$–8.2 mm were then repeated with these fixed values C_P and C_S. The resulting capacitive power P_C and inductive power P_I during the power pulse are shown in Fig. 11.

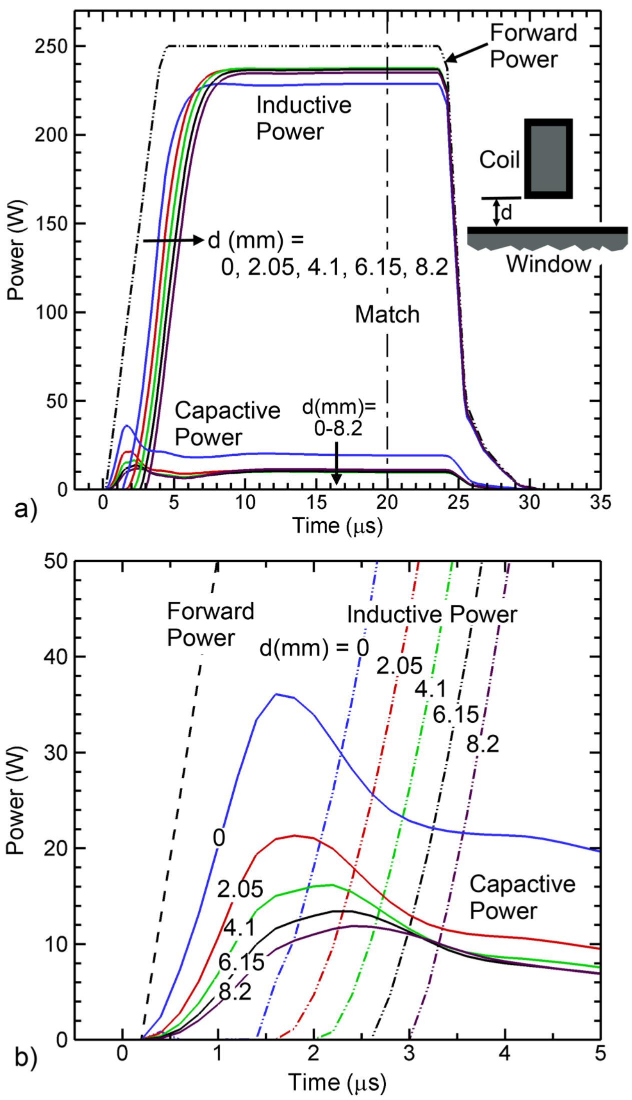

FIG. 11. Inductive and capacitive power deposition for different gaps, d, between the coils and the top of the dielectric window. Heights range between $d = 0$ and 8.2 mm. (a) Power over the entire power-on period and (b) power during the first $5\,\mu$s. The circuit match values correspond to the match time $t_M = 20\,\mu$s (Ar/Cl_2 = 65/35, 25 mTorr, PRF = 13.3 kHz, DC = 35%, P_S = 250 W).

With increasing values of the gap, d, the series capacitance of the gap–window pair decreases. With $d = 0$ (maximum capacitance), E-mode power is dissipated at the leading edge of the power pulse. This capacitive power produces ionization, which then enables the inductive power to begin earlier leading to an onset of the H-mode. As the gap size d increases, the series capacitance also decreases. This decrease in capacitance of the gap limits current, which then decreases the E-mode power at the leading edge of the power pulse and increases the reflection coefficient. With lower E-mode power deposition, the increase in electron density is slower. This slow rate of increase in electron density means that more time is required for the electron density to increase to the point that inductive power dominates and the H-mode begins. During the quasi-steady state portion of the pulse where the circuit is well matched to the plasma, the small values of d allow for larger capacitive power deposition, which then reduces the inductive power deposition.

For all values of the antenna–window gap, there is nearly a perfect match late in the pulse—all forward power is dissipated either in the plasma or in the antenna. However, the manner of deposition, fraction of power dissipated as P_C and P_I, is sensitive to the height of the antenna above the window. In results not shown here, there is a similar dependence on the flatness of the antenna. An antenna that may be mounted at a small angle with respect to the window can be perfectly matched; however, the fractions of power dissipated as P_C and P_I are a function of the orientation of the antenna. Reproducing performance when replacing an antenna requires both ensuring a match and also reproducing the fraction of power separately dissipated as P_C and P_I. In the case of pulsed plasmas, the power waveforms should also be reproduced.

F. Electrostatic waves at the onset of the E-mode

For thermally attaching gas mixtures, as in the Ar/Cl_2 mixture used in this investigation, the onset of the E-mode at the leading edge of the power pulse produces an impulsive perturbation to the plasma that generates electrostatic waves. At the beginning of the power pulse, the plasma is essentially an ion–ion plasma with the positive and negative ion densities greatly exceeding the electron density. For example, for the base case at the end of the afterglow, the positive and negative ion densities adjacent to the window are essentially equal at 3.4×10^{10} cm^{-3}, whereas the electron density is 2×10^{8} cm^{-3}. The charge density (units of elementary charge, q = 1.6×10^{-19} C) is -2.5×10^{4} cm^{-3}. There essentially is no sheath as both positive ions have largely thermalized to the same temperature during the afterglow and the ions have nearly the same mobilities.

When the power is applied, a large voltage is generated across the antenna and capacitive coupling to the plasma occurs. The response of the plasma is to attempt to form a sheath to dissipate the capacitive voltage drop. During the first few RF cycles, the sheath is most easily formed by accelerating electrons adjacent to the dielectric into the plasma to produce a positive space charge region. During these first few cycles, the far more numerous positive and negative ions are nearly immobile and do not significantly separate to produce the charge density needed to create the sheath. With each half cycle, electrons are expelled from and attracted to the dielectric. The end result is the launching of electrostatic waves into the ion–ion plasma.

The electron and charge density are shown in Fig. 12 during the first six cycles of the power pulse for the base case with a match point of $t_M = 1.5\,\mu$s. These conditions were chosen to emphasize the initial E-mode coupling for demonstration purposes. The electron density is shown as color contours. The charge density ρ (units of elementary charge/cm^3) is shown with numerical labels with a line for ρ = 0 indicating a sign change in the local charge density. As the power increases at the beginning of the pulse, the voltage on the coils increases with each successive RF cycle. Electrons adjacent to all surfaces in contact with the plasma are expelled into the plasma in an attempt to form a sheath. This expulsion is most pronounced under the window adjacent to the coils but also occurs along the sidewalls and substrate. The expulsion first produces an electrostatic wave having ρ < 0. Since the electron density is two orders of magnitude less than the positive and negative ions, this wave can propagate through the plasma without significantly perturbing the overall charge balance. The anodic half of the cycle launches a positive electrostatic wave. With each cycle, a new wave is launched, producing layers of alternating charge propagating into the plasma. The waves appear to emanate from under the inner and middle coils where the voltage is the largest and the largest amount of charge must be expelled to form the sheath.

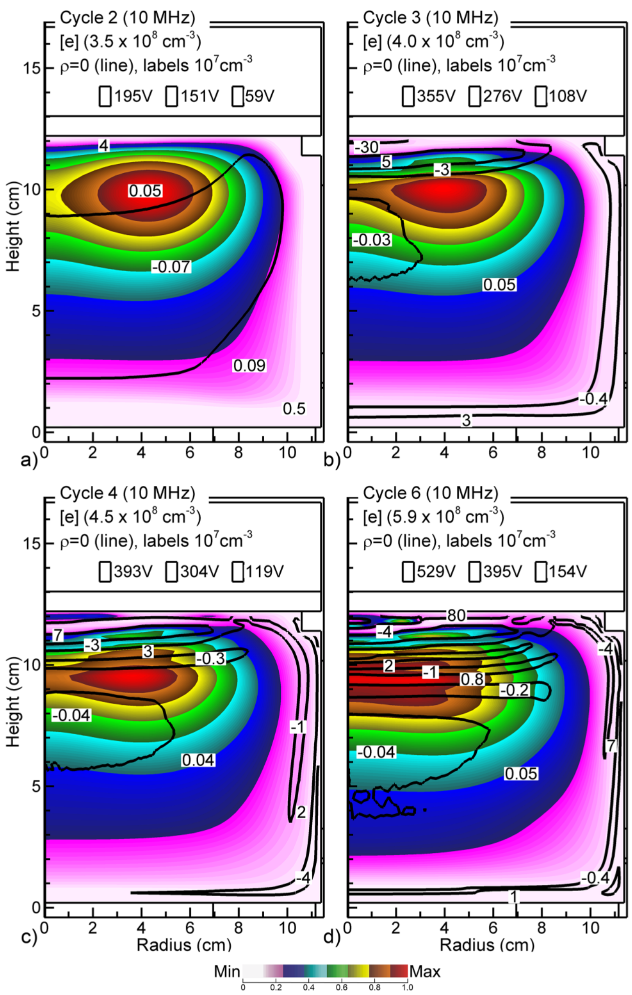

FIG. 12. Electron density (color contours) and charge density over the first few RF cycles of a pulsed period. (a) Second, (b) third, (c) fourth, and (d) sixth cycles. The circuit match values correspond to the match time $t_M = 1.5\,\mu$s. The charge density ρ is shown by labels in units of 10^7q (1.6×10^{-19} C)/cm^3 with a line denoting ρ = 0 (Ar/Cl_2 = 65/35, 25 mTorr, PRF = 13.3 kHz, DC = 35%, P_S = 250 W). The impulsive power deposition launches electrostatic waves.

In time, the electron density increases and positive space charge sheath is formed under the dielectric while the initial electrostatic waves collisionally dissipate. The waves soon become chaotic (not shown) due to the disparity in coil voltages, each with slightly different phases. The oscillating voltage on each coil launches what appears to be a cylindrically expanding electrostatic wave of different magnitude. These individually expanding waves are close enough in phase that their sum appears to have only a slight curvature. However, on successive pulses, the disparity in voltage between the coils increases, producing expanding waves that intersect and become chaotic before dissipating.

These electrostatic waves will occur in any highly electronegative system in which a sharply rising negative voltage is applied to a surface. For example, in pulsed plasma doping (P^{2}LAD) systems, a multi-kV negative, nearly step-function pulse is applied to the substrate to accelerate ions into the wafer for shallow junction implantation.[39] Simulations of P^{2}LAD systems predict similar electrostatic waves, albeit more soliton-like due to the single transient voltage.[40] In the ICP systems discussed here, the amplitude and duration of the waves are small, and so the effects on processing (e.g., etch rate or uniformity) are likely not large. Their effects on diagnostics and sensors could be problematic, particularly if the waves are not reproducible pulse-to-pulse.

IV. CONCLUDING REMARKS

Power dissipation in CW and pulsed electronegative inductively coupled plasmas sustained in Ar/Cl_2 mixtures and the consequences of impedance matching were computationally investigated. During a pulsed cycle, the modulation in electron density determines the mode of power deposition—capacitive (E-mode) at low electron density where the electromagnetic skin depth is large, and inductive (H-mode) at high electron density where the electromagnetic skin is small. Even with perfect power transfer from the supply to the plasma, there is a natural E–H-mode that occurs at the beginning of the pulsed period.

When considering matching, the increase in plasma density and spatial distribution of the plasma changes the impedance of the plasma reactor during pulsing, which then changes the matching requirements to deliver power from the supply. Since components in the match box are typically fixed during the pulsed period, components in the match box are set to match the plasma at particular times during the pulsed period. If the matchbox is chosen to match the impedance at the onset of the power pulse, the E-mode is emphasized and a fast plasma ignition is expected due to efficient power deposition during power ramp-up. However, the trade-off is a high power reflection coefficient during the majority of the power-on period as a consequence of the impedance mismatch to the H-mode plasma. In contrast, matching the higher power H-mode produces more net power transfer from the supply to the plasma but delays the onset of the H-mode due to the mismatch of power in the E-mode.

Duty cycle during pulsing has important implications on power matching. In general, the shorter the duty cycle, the lower the electron density at the beginning of the next power pulse. This is particularly the case for mixtures using gases that attach thermal electrons, such as Cl_2. The lower electron density with a shorter duty cycle promotes the E-mode operation at the start of the next power pulse.

In highly electronegative gases, the plasma at the beginning of the power pulse is essentially an ion–ion plasma. The impulsive application of power in purely an E-mode results in launching of electrostatic waves during the leading RF cycles. The response of the plasma to the high voltage on the antenna during the E-mode is to form a sheath. The electrostatic waves result from the expulsion of the remaining electrons from nearby surfaces in an attempt to form a sheath. These waves are more severe when the afterglow is long and electronegativity is high.

Capacitance is largely a function of geometry and so the capacitance between the antenna and the plasma is a function of the gap length between the coil and dielectric window. A big gap produces a small capacitance and decreases the capacitive power that can be deposited during the E-mode. That decrease in power reduces the initial increase in electron density, which then delays the onset of the H-mode.

Power matching to transient systems will be challenging as long as the matching requires mechanical changes in components. These mechanical changes simply cannot be made rapidly enough to track the change in plasma impedance. As pulsed plasmas become even more prevalent in semiconductor manufacturing, advanced matching techniques, such as frequency tuning, will be required to minimize mode transitions and instabilities.

ACKNOWLEDGMENTS

This work was supported by Samsung Electronics Ltd., Lam Research Inc., and the National Science Foundation (No. PHY-1902878). This material was also based on the work supported by the U.S. Department of Energy, Office of Sciences Fusion Energy Sciences under Award Nos. DE-SC000319, DE-SC0020232, and DE-SC0014132.

APPENDIX: PERFECT MATCH VALUES OF C_P AND C_S

For parametric studies, it is desirable to have a perfect match between the power supply and the plasma reactor. The method of solution to obtain the perfect match values of C_P and C_S are described in this Appendix. For the circuit architecture shown in Fig. 1, the input impedance to the matchbox is given by

$$Z_M = R_M + \frac{1}{j\omega C_S} + \frac{1}{\dfrac{1}{j\omega L_p + \dfrac{1}{j\omega C_p}} + \dfrac{1}{\mathrm{Re}(Z_L) + j\,\mathrm{Im}(Z_L)}}.$$

To obtain the perfect match, we need to have $\mathrm{Re}(Z_M) = Z_0$, and $\mathrm{Im}(Z_M) = 0$. Define

$$A = [\mathrm{Re}(Z_0) - R_M]\left\{|Z_L|^2\omega^4 L_p^2 + \omega^2|Z_L|^4 + 2\omega^3 L_p\,\mathrm{Im}(Z_L)|Z_L|^2\right\} - \mathrm{Re}(Z_L)\omega^4 L_p^2|Z_L|^2,$$

$$B = 2\omega^2 L_p\,\mathrm{Re}(Z_L)|Z_L|^2 - 2\omega|Z_L|^2[\mathrm{Re}(Z_0) - R_M][\omega L_p + \mathrm{Im}(Z_L)],$$

$$C = \{[\mathrm{Re}(Z_0) - R_M] - \mathrm{Re}(Z_L)\}|Z_L|^2,$$

where $|Z_L|$ is the magnitude of Z_L. With these values,

$$C_P = \frac{-B \pm \sqrt{B^2 - 4AC}}{2A},$$

$$C_S = -\frac{\mathrm{Re}(Z_L)^2(1-\omega^2 L_p C_p)^2 + [\omega C_p|Z_L|^2 - \mathrm{Im}(Z_L)(1-\omega^2 L_p C_p)]^2}{\omega(1-\omega^2 L_p C_p)|Z_L|^2[\omega C_p|Z_L|^2 - \mathrm{Im}(Z_L)(1-\omega^2 L_p C_p)]}.$$

The positive value of C_P is chosen.

REFERENCES

[1]P. Chabert, J. L. Raimbault, J. M. Rax, and M. A. Lieberman, Phys. Plasmas **11**, 1775 (2004).
[2]J. Gudmundsson and M. A. Lieberman, Plasma Sources Sci. Technol. **7**, 83 (1998).
[3]K. Kurokawa, IEEE Trans. Microw. Theory Tech. **13**, 194 (1965).
[4]S. Xu, K. N. Ostrikov, Y. Li, E. L. Tsakadze, and I. R. Jones, Phys. Plasmas **8**, 2549 (2001).
[5]F. Schmidt, J. Schulze, E. Johnson, J. Booth, D. Keil, D. M. French, J. Trieschmann, and T. Mussenbrock, Plasma Sources Sci. Technol. **27**, 095012 (2018).
[6]J. Franek, S. Brandt, B. Berger, M. Liese, M. Barthel, E. Schüngel, and J. Schulze, Rev. Sci. Instrum. **86**, 053504 (2015).
[7]T. Mussenbrock, R. P. Brinkmann, M. A. Lieberman, A. J. Lichtenberg, and E. Kawamura, Phys. Rev. Lett. **101**, 085004 (2008).
[8]J. Schulze, B. G. Heil, D. Luggenhölscher, R. P. Brinkmann, and U. Czarnetzki, J. Phys. D Appl. Phys. **41**, 195212 (2008).
[9]L. Liu, S. Sridhar, V. M. Donnelly, and D. J. Economou, J. Phys. D Appl. Phys. **48**, 485201 (2015).
[10]C. Xue, D. Wen, W. Liu, Y. Zhang, F. Gao, and Y. Wang, J. Vac. Sci. Technol. A **35**, 021301 (2017).
[11]T. Wegner, C. Küllig, and J. Meichsner, Plasma Sources Sci. Technol. **26**, 025006 (2017).
[12]T. Wegner, C. Küllig, and J. Meichsner, Plasma Sources Sci. Technol. **26**, 025007 (2017).
[13]J. Wang, Y. Du, X. Zhang, Z. Zheng, Y. Liu, L. Xu, P. Wang, and J. Cao, Phys. Plasmas **21**, 073502 (2014).

[14]M. A. Lieberman and A. J. Lichtenberg, *Principles of Plasma Discharges and Materials Processing*, 2nd ed. (John Wiley & Sons, Inc., Hoboken, NJ, 2005).
[15]P. Chabert and N. Braithwaite, *Physics of Radiofrequency Plasmas* (Cambridge University Press, Cambridge, 2011).
[16]S. V. Singh and C. Pargmann, J. Appl. Phys. **104**, 083303 (2008).
[17]T. Gans, M. Osiac, D. O'Connell, V. A. Kadetov, U. Czarnetzki, T. Schwarz-Selinger, H. Halfmann, and P. Awakowicz, Plasma Phys. Controlled Fusion **47**, A353 (2005).
[18]G. Cunge, B. Crowley, D. Vender, and M. M. Turner, Plasma Sources Sci. Technol. **8**, 576 (1999).
[19]M. Lee and C. Chung, Plasma Sources Sci. Technol. **19**, 015011 (2010).
[20]M. M. Turner and M. A. Lieberman, Plasma Sources Sci. Technol. **8**, 313 (1999).
[21]T. Czerwiec and D. B. Graves, J. Phys. D Appl. Phys. **37**, 2827 (2004).
[22]T. Wegner, C. Küllig, and J. Meichsner, Plasma Sources Sci. Technol. **24**, 044001 (2015).
[23]P. Chabert, A. J. Lichtenberg, M. A. Lieberman, and A. M. Marakhtanov, Plasma Sources Sci. Technol. **10**, 478 (2001).
[24]U. Kortshagen, N. D. Gibson, and J. E. Lawler, J. Phys. D Appl. Phys. **29**, 1224 (1996).
[25]E. Despiau-Pujo and P. Chabert, Plasma Sources Sci. Technol. **18**, 045028 (2009).
[26]C. Chung and H. Chang, Appl. Phys. Lett. **80**, 1725 (2002).
[27]P. Kempkes, S. V. Singh, C. Pargmann, and H. Soltwisch, Plasma Sources Sci. Technol. **15**, 378 (2006).
[28]E. Kawamura, M. A. Lieberman, A. J. Lichtenberg, and D. B. Graves, Plasma Sources Sci. Technol. **21**, 045014 (2012).
[29]M. Lee and C. Chung, Phys. Plasmas **13**, 063510 (2006).
[30]A. M. Daltrini, S. A. Moshkalev, T. J. Morgan, R. B. Piejak, and W. G. Graham, Appl. Phys. Lett. **92**, 061504 (2008).
[31]M. J. Kushner, J. Phys. D **42**, 194013 (2009).
[32]P. Tian and M. J. Kushner, Plasma Sources Sci. Technol. **26**, 024005 (2017).
[33]M. J. Kushner, W. Z. Collison, M. J. Grapperhaus, J. P. Holland, and M. S. Barnes, J. Appl. Phys. **80**, 1337 (1996).
[34]R. B. Piejak, V. A. Godyak, and B. M. Alexandrovich, Plasma Sources Sci. Technol. **1**, 179 (1992).
[35]T. Ohba, W. Yang, S. Tan, K. J. Kanarik, and K. Nojiri, Jpn. J. Appl. Phys. **56**, 06HB06 (2017).
[36]D. J. Coumou, S. T. Smith, D. J. Peterson, and S. C. Shannon, IEEE Trans. Plasma Sci. **47**, 2102 (2019).
[37]D. Metzler, C. Li, S. Engelmann, R. L. Bruce, E. A. Joseph, and G. S. Oehrlein, J. Vac. Sci. Technol. A **34**, 01B101 (2016).
[38]S. J. Lanham and M. J. Kushner, "Investigating mode transitions in pulsed inductively coupled plasmas," in *64th American Vacuum Society International Symposium, Tampa, FL, November 2017* (American Vacuum Society, 2017), Paper PS-WeA10.
[39]S. B. Felch, Z. Fang, B.-W. Koo, R. B. Liebert, S. R. Walther, and D. Hacker, Surf. Coat. Technol. **156**, 229 (2002).
[40]A. Agarwal and M. J. Kushner, J. Appl. Phys. **101**, 063305 (2007).